PCP
PLANT & CELL PHYSIOLOGY

An IQ Domain Mediates the Interaction with Calmodulin in a Plant Cyclic Nucleotide-Gated Channel

Cornelia Fischer[1], Annette Kugler[1,2], Stefan Hoth[1,3] and Petra Dietrich[1,*]

[1]Molekulare Pflanzenphysiologie and Erlangen Center of Plant Science, Department Biology, Friedrich-Alexander-Universität Erlangen-Nürnberg, Staudtstraße 5, D-91058 Erlangen, Germany
[2]Present address: Department of Plant Sciences, University of Oxford, South Parks Road, Oxford OX1 3RB, UK.
[3]Present address: Molekulare Pflanzenphysiologie, Universität Hamburg, Biozentrum Klein Flottbek, Ohnhorststraße 18, D-22609 Hamburg, Germany.
*Corresponding author: E-mail, dietrich@biologie.uni-erlangen.de; Fax, +49-9131-8528751.
(Received November 22, 2012; Accepted January 28, 2013)

Regular Paper

Cyclic nucleotide-gated channels (CNGCs) form non-selective cation entry pathways regulated by calmodulin (CaM), a universal Ca^{2+} sensor in eukaryotes. Although CaM binding has been shown to be important for Ca^{2+}-dependent feedback regulation of CNGC activity, the CaM-binding properties of these channels have been investigated in a few cases only. We show that CNGC20 from *Arabidopsis thaliana* binds CaM in a Ca^{2+}-dependent manner and interacts with all AtCaM isoforms but not with the CaM-like proteins CML8 and CML9. CaM interaction with the full-length channel was demonstrated in planta, using bimolecular fluorescence complementation. This interaction occurred at the plasma membrane, in accordance with our localization data of green fluorescent protein (GFP)-fused CNGC20 proteins. The CaM-binding site was mapped to an isoleucine glutamine (IQ) motif, which has not been characterized in plant CNGCs so far. Our results show that compared with the overlapping binding sites for cyclic nucleotides and CaM in CNGCs studied so far, they are sequentially organized in CNGC20. The presence of two alternative CaM-binding modes indicates that ligand regulation of plant CNGCs is more complex than previously expected. Since the IQ domain is conserved among plant CNGCs, this domain adds to the variability of Ca^{2+}-dependent channel control mechanisms underlining the functional diversity within this multigene family.

Keywords: Arabidopsis • Calcium • Calmodulin • CNGC • IQ domain • Nuclear localization sequence.

Abbreviations: BiFC, bimolecular fluorescence complementation; CaM, calmodulin; CaMBD, calmodulin-binding domain; CML, calmodulin-like protein; CNBD, cyclic nucleotide-binding domain; CNGC, cyclic nucleotide-gated channel; GFP, green fluorescent protein; MBP, maltose-binding protein; NLS, nuclear localization sequence; PI, propidium iodide; VC, Venus C-terminus, VN, Venus N-terminus; YTH, yeast two-hybrid.

Introduction

Ca^{2+} plays a fundamental role as a second messenger in living cells. Signaling information is encoded by temporal and spatial dynamics of the Ca^{2+} concentration, which is sensed via several Ca^{2+}-binding proteins and subsequently transduced by these sensors (sensor responder) or their interacting targets in a 'sensor relay system' (Sanders et al. 2002, Dodd et al. 2010). Three major classes of Ca^{2+} sensor relay systems have been found. Plant-specific calcineurin B-like proteins (CBLs) couple to the CBL-interacting kinases (CIPKs), while calmodulins (CaMs) and CaM-like proteins (CMLs) address different types of target proteins. In Arabidopsis, four CaM isoforms are built from seven CaM genes, each equipped with four conserved Ca^{2+}-binding EF-hands (McCormack et al. 2005). In addition, about 50 CMLs are found, which share 16–75% amino acid identity with CaM2 (McCormack et al. 2003, DeFalco et al. 2010). In Arabidopsis, >100 target enzymes for CaM and CMLs have been identified experimentally or predicted according to homology (Reddy et al. 2002, Bouché et al. 2005, Popescu et al. 2007).

Within its target proteins, CaM binds to CaM-binding domains (CaMBDs), which are not necessarily conserved in their sequence albeit that they share some common structural and physico-chemical characteristics. The CaMBD is generally composed of 16–30 amino acids, which may adopt an amphipathic α-helical structure with basic and hydrophobic faces (O'Neil et al. 1990, Yamniuk et al. 2004). A bulky hydrophobic residue is located near each end of the domain. Depending on the distance between these hydrophobic residues, the CaM-binding, 1-10, 1-12, 1-14 or 1-16 motifs are distinguished (Rhoads et al. 1997). Although putative CaMBDs may be predicted according to these characteristics (The Calmodulin Target Database; calcium.uhnres.utoronto.ca), many proteins containing a putative CaMBD do not bind CaM and many CaMBDs of known CaM targets remain unknown (Rhoads et al. 1997, Yamniuk et al. 2004).

Plant Cell Physiol. 54(4): 573–584 (2013) doi:10.1093/pcp/pct021, available online at www.pcp.oxfordjournals.org
© The Author 2013. Published by Oxford University Press on behalf of Japanese Society of Plant Physiologists.
This is an Open Access article distributed under the terms of the Creative Commons Attribution Non-Commercial License (http://creativecommons.org/licenses/by-nc/3.0/), which permits unrestricted non-commercial use, distribution, and reproduction in any medium, provided the original work is properly cited.

Besides the 1-10 to 1-16 motifs, CaM target proteins with CaMBDs of conserved amino acid sequences have been identified. This conventional isoleucine–glutamine (IQ) motif IQxxxRGxxxR, where x denotes any residue (Rhoads et al. 1997), was first identified in a few proteins, but a more generalized version, [MFILV]QxxxRxxxx[RK], was developed from additional CaMB targets (Bähler et al. 2002). Often, 2–3 conserved alanine residues are found N-terminally to the primary motif. In general, the IQ domain encompasses 20–25 residues and exhibits the potential to adopt an α-helical conformation that is stabilized in the presence of CaM. IQ motifs have been investigated in detail in animal proteins, which often bind Ca^{2+}-free CaM (apoCaM) while Ca^{2+} induces the displacement of the CaM ligand (Rhoads et al. 1997). On the other hand, IQ domains present in, for example, the voltage-dependent L-type calcium channels (Ca_V1) require Ca^{2+} for interaction with CaM and subsequent channel inactivation (Peterson et al. 1999, Pate et al. 2000). The functions of IQ domains in plant proteins have not been investigated in detail, despite their presence in, for example, myosins, the IQ domain (IQD) family, the CaM-binding transcriptional activators (CAMTAs) and cyclic nucleotide-gated channels (CNGCs) (Bähler et al. 2002, Reddy et al. 2002, Abel et al. 2005).

CNGCs are involved in diverse physiological functions, such as plant growth, adaptation to elevated Ca^{2+} concentrations and responses to abiotic and biotic stresses (Clough et al. 2000, Chan et al. 2003, Kaplan et al. 2007, Chin et al. 2009, Dietrich et al. 2010). CNGCs belong to the superfamily of ion channels with six transmembrane domains and are assumed to function as tetramers, with each subunit contributing to the formation of the cation-selective pore. Thus, depending on the pore properties and heteromer formation, multiple functional channels with a different ion selectivity and activity pattern will arise. Unfortunately, the lack of detailed functional expression studies on these cation channels limits current knowledge about their permeation properties and ligand-dependent gating. Within the carboxyl tail of the proteins, a conserved binding domain for cyclic nucleotides (CNBD) is exposed to the cytosol, which includes four α-helices and eight β-sheets (Kaplan et al. 2007). In addition, the carboxyl tail of several plant CNGCs has been shown to bind CaM in a Ca^{2+}-dependent manner (Schuurink et al. 1998, Arazi et al. 2000a, Köhler et al. 2000, Reddy et al. 2002). In CNGC1, the CaM-binding site has been mapped (Köhler et al. 2000) and corresponds to the last αC-helix of the CNBD. A homologous region in CNGC2 mediated interaction with CaM4 (Hua et al. 2003). Finally, a peptide representing the αC-helix of the tobacco CaM-binding protein NtCBP4 displayed high-affinity CaM binding characteristics with a K_d of 8 nM (Arazi et al. 2000a).

Because of the partial overlapping CNBD and CaMBD, a competitive regulation by cyclic nucleotides and CaMs was anticipated (Arazi et al. 2000b) and experimentally verified for CNGC2 (Hua et al., 2003). Accordingly, current models for the regulation of plant CNGCs imply the binding of a cyclic nucleotide (cAMP or cGMP) to the CNBD prior to channel opening. Interaction with CaM is favored in the presence of elevated Ca^{2+} concentrations, leading to displacement of the cyclic nucleotide and channel closure (Arazi et al. 2000b, Kaplan et al. 2007).

In total, the Arabidopsis CNGC gene family contains 20 members subdivided into five groups (Mäser et al. 2001), whereas CaM binding has only been investigated in detail for CNGC1 belonging to group I and for CNGC2 from group IVB (Köhler et al. 2000, Hua et al. 2003). Since the above-described functional diversity of these channels may in part be related to their CaM-binding properties, we selected CNGC20 for interaction studies, a salt-regulated channel expressed in guard cells, older leaves and in roots (Kugler et al. 2009). While the highest expression of CNGC20 is predominantly found in older leaves, where it is expressed in mesophyll cells, epidermal cells and guard cells, CNGC19 is mainly expressed in the vascular tissues (Kugler et al. 2009), rendering a heteromer formation unlikely. In contrast, heteromer formation of CNGC20, CNGC2 and CNGC4 appears more likely due to overlapping expression mainly in the shoot.

In addition to salinity stress, array analyses have revealed that this channel gene is up-regulated upon UV-B but not heat or drought stress (Kilian et al. 2007). Like several other CNGCs including CNGC2 (Clough et al. 2000, Yu et al. 2000), CNGC20 is also involved in responses to pathogen attack. A transient increase in transcript abundance was detected within hours following treatment with the pathogen-associated molecular pattern (PAMP) molecules flg22 and HrpZ (Winter et al. 2007). In contrast, long-term pathogen responses included the down-regulation of CNGC20, during the weeks of nematode infestation (Hammes et al. 2005), and following infection by the *Cabbage leaf curl virus* (Ascencio-Ibanez et al. 2008). Together with CNGC19, CNGC20 constitutes group IVA of the CNGC family, and both channels form a quantitative trait locus with impact on accumulation of cesium ions (Kanter et al. 2010). CNGC20 is only distantly related to CNGC1 and CNGC2, with 31% and 28% identity, respectively, for which CaM binding has been shown.

Our results highlight a new mode of CaM interaction in plant CNGCs and underline the functional diversity within this gene family.

Results

CNGC20 interacts with calmodulins rather than calmodulin-like proteins

We used the C-terminus of CNGC20 (CNGC20-C) to study its interaction with CaM isoforms and CMLs in pairwise yeast two-hybrid (YTH) interaction assays. This approach allowed the qualitative and quantitative analysis of the interaction, resulting in His auxotrophic growth and transactivation of a β-galactosidase gene (**Fig. 1**). Co-expression of CNGC20-C as a bait (BD-CNGC20-C) and CaM2 (identical to 3 and 5), 4 (identical to 1), 6, and 7 as prey (AD-CaM) enabled yeast

 © The Author 2013.

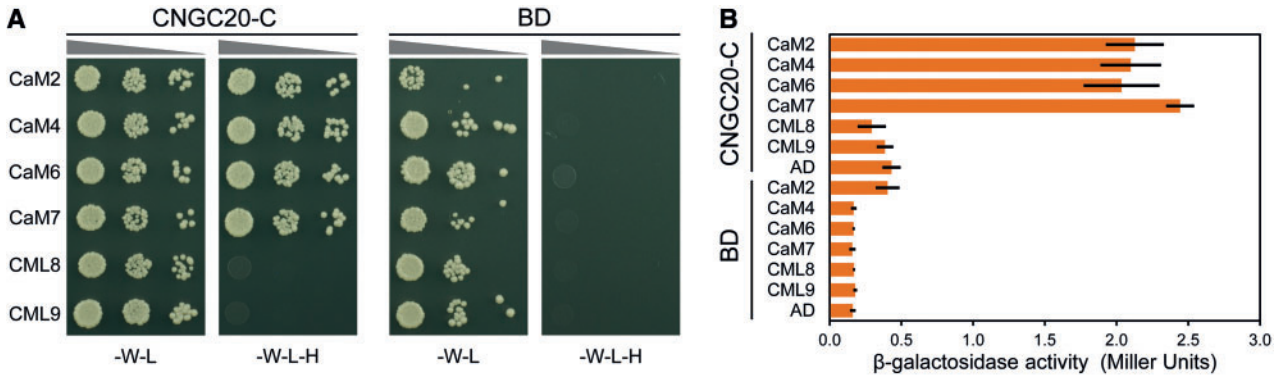

Fig. 1 The C-terminus of CNGC20 interacts with calmodulins but not calmodulin-like proteins. (A) Left columns: the CNGC20 C-terminus (CNGC20-C) fused to the GAL4-binding domain (BD) was used in the YTH assay together with CaM isoforms or the CaM-like proteins CML8 and CML9, which were fused to the GAL4-activation domain (AD). Right columns: experiments repeated using the BD without CNGC20-C. Yeasts were grown in the absence of tryptophan (−W) and leucine (−L) for selection of co-transformed cells, and in the absence of histidine (−H), tryptophan (−W) and leucine (−L) to monitor protein interactions. (B) Interaction between CNGC20-C and CaM isoforms, CML8 and CML9 was quantified using the β-galactosidase activity assay. Bars represent mean results of two independent measurements with three replicates each. Labels as in (A).

growth in the absence of His, demonstrating that all four CaM isoforms represent putative interaction partners of CNGC20 (**Fig. 1A**). The strength of the interaction was quantified as relative β-galactosidase activities, showing robust interaction for all CaM isoforms (**Fig. 1B**). These CaM isoforms constitute group 1 of the CaM/CML family in Arabidopsis and share ≥96% amino acid identity (McCormack et al. 2003). The two most related CML isoforms are those of group 2. We therefore chose two members of this group, CML8 with 73% identity, and CML9 with 50% identity to CaM2. CML8 and CML9 were previously used for interaction studies with CNGC1 and 2 (Köhler et al. 2000), providing a basis for comparability of the CaM selectivity among different CNGCs. Like CNGC20, CML9 is up-regulated upon salinity stress and PAMP treatment (Magnan et al. 2008, Leba et al. 2012), and CML9 knockout mutants are characterized by an enhanced tolerance to salt stress. However, no interaction was found for the CaM-like proteins CML8 and CML9 (**Fig. 1**).

Mapping of the calmodulin interaction domain

To map the CaM interaction domain within CNGC20, we investigated binding capacities of different truncated C-terminal fragments. **Fig. 2A** illustrates the C-terminus including the α-helices and β-sheets present within the CNBD of CNGC20 and derived peptides used in the YTH assays. When the last 63 amino acids were deleted from the C-terminus of CNGC20 (CNGC20-C-ΔC63), interaction was not observed for CaMs or for CMLs (**Fig. 2B**). The re-addition of 29 amino acids of the channel's C-terminus including the region homologous to the previously identified CaMBD (Arazi et al. 2000a, Köhler et al. 2000) was also not able to restore the interaction with CaM isoforms in CNGC20-C-ΔC34 (**Fig. 2C**). These results show that essential parts for the establishment of the CaM contact are likely to be provided by the last 34 amino acids. Indeed, a peptide representing the last 34 amino acids (CNGC20-CC) was able to interact with all four CaM isoforms but not with CML8 and CML9 (**Fig. 2D**), as was the case with the complete C-terminus. Thus, in CNGC20, CaM interacts with a region downstream of the CNBD, behavior different from that of other CNGCs (Arazi et al. 2000a, Köhler et al. 2000, Hua et al. 2003). The lack of interaction with CaM was also observed for a peptide including the αB and αC helices (CNGC20-αBC, **Fig. 2E**). In a previous report (Arazi et al. 2000a), a tetrapeptidic stretch following the αC-helix (WRTW) was shown to be important for high-affinity CaM binding of NtCBP4. However, in CNGC20, a peptide including the αC-helix and the corresponding residues WRLR did not induce CaM binding in CNGC20-αC (**Fig. 2F**). These results confirm that the last 34 amino acids of CNGC20 are sufficient to establish the full CaM interaction activity of the entire C-terminus. Additional CaM-binding activity within the C-terminus does not exist, because all fragments excluding the last 34 amino acids were unable to interact. While the CaMBD overlaps with the CNBD in plant CNGCs studied so far, these two ligand interaction domains are sequentially organized in CNGC20.

Calmodulin interacts with an IQ domain in a Ca^{2+}-dependent manner

An alignment of part of the C-termini from plant CNGCs is shown in **Fig. 3A**. Within the αC-helix of the CNBD, an unclassified database CaMBD is found in CNGC1, CNGC2, CNGC3, CNGC4, HvCBT1 and NtCBP4 (calcium.uhnres.utoronto.ca). CaM binding to this region has been experimentally verified for CNGC1, CNGC2 and NtCBP4 (Arazi et al. 2000a, Köhler et al. 2000, Hua et al. 2003). Although the homologous region in CNGC20 is also predicted to form a CaM-binding site (calcium.uhnres.utoronto.ca), this region corresponding to the αC-helix of the CNBD of CNGC20 did not interact with CaMs (**Fig. 2**).

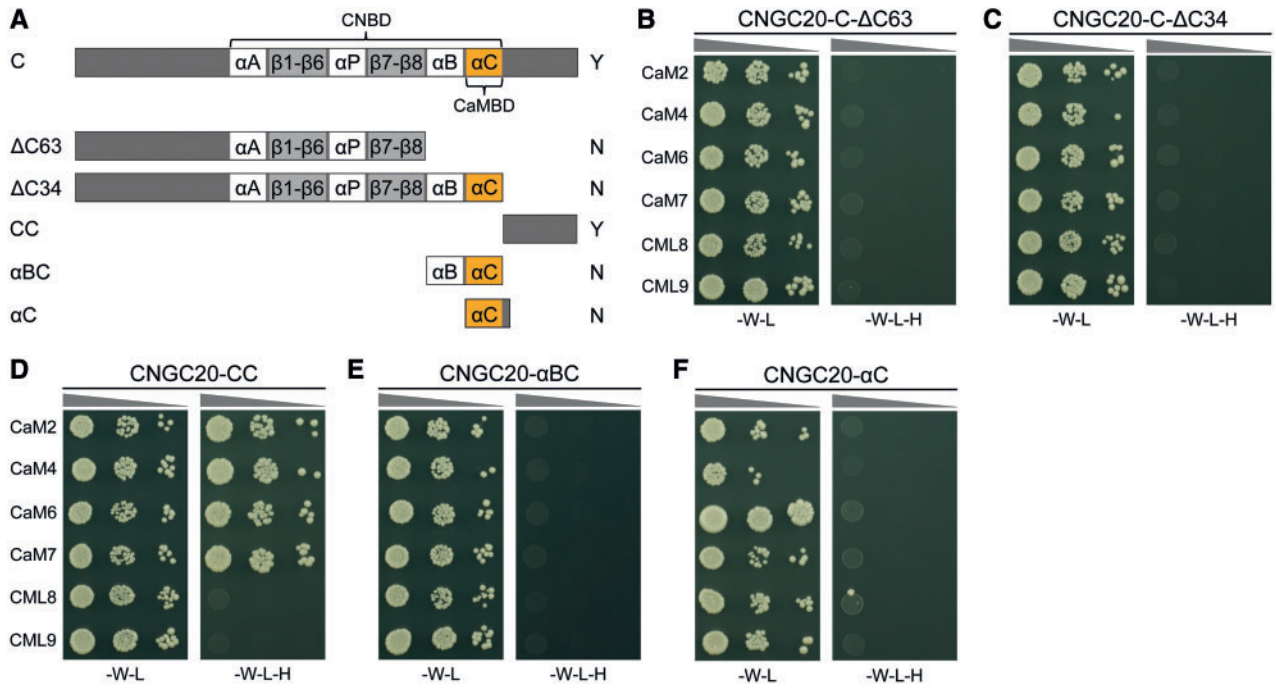

Fig. 2 The CaM-binding domain in CNGC20 maps outside of the CNBD. (A) Schematic illustration of CNGC20 peptides used in YTH assays. Gray bars represent the C-terminus of CNGC20 including the CNBD with eight β-sheets (light gray boxes), three α-helices (white boxes) and the last α-helix (orange, αC) as predicted for the CaMBD. The nomenclature of peptides is explained in the text. Y and N indicate positive and negative interaction results from YTH experiments, respectively. (B–F) Growth results from YTH interaction assays as described in **Fig. 1**, using peptides as depicted in (A): (B) CNGC20-C-ΔC63 lacking the last 63 residues; (C) CNGC20-C-ΔC34 lacking the last 34 amino acids; (D) CNGC20-CC representing the last 34 amino acids without the predicted αB- and αC-helices of the CNBD was able to interact with CaMs; (E and F) a fragment containing the αB- and αC-helix (αBC) did not interact with CaMs (E) nor could the extension of the αC helix (αC) to the motif WRLR restore CaM interaction (F).

Interestingly, an additional α-helical structure following the CNBD is predicted in CNGC20 (R734-L755, Rost et al. 2004), which is located almost at the very end of the 764 amino acid long channel protein. Within this region, an IQ motif is present within all plant CNGCs (**Fig. 3A**; Abel et al. 2005). IQ domains have been shown to interact with EF-hand-containing proteins and therefore represent likely targets for CaM interaction (Bähler et al. 2002). Indeed, a stretch of only 16 amino acids (AARQIQVAWRYRRRRL) corresponding to the IQ domain (CNGC20-IQ) was able to interact with all Arabidopsis CaM isoforms (**Fig. 3B**).

While the YTH method was suited to demonstrate interaction with CaMs in vivo and to map the responsible CaMBD, the calcium concentration during the interaction is unknown. The calcium dependence of the interaction was investigated using a CaM overlay assay, and it was demonstrated that the interaction of CaM2 with CNGC20-C required the presence of Ca^{2+} (**Fig. 3C**).

CNGC20 is localized in the plasma membrane and interacts with calmodulin in vivo

Green fluorescent protein (GFP) and mCherry fusion proteins were used to monitor the cellular distribution of CNGC20 and CaM2 proteins, respectively. GFP fluorescence was detected in the plasma membrane of mesophyll protoplasts and epidermal cells of *Nicotiana benthamiana* expressing a CNGC20–GFP fusion protein (**Fig. 4A–C**). Similarly, an N-terminal fusion of GFP resulted in plasma membrane localization of GFP–CNGC20 (**Fig. 4D**). In addition to the plasma membrane localization, we frequently observed punctuate structures within cells exhibiting strong expression (**Fig. 5A**). As fluorescence from CNGC–GFP fusion proteins can be observed along the secretory pathway to the plasma membrane (Christopher et al. 2007), these dots may highlight the involved organelles.

Upon co-expression of CNGC20–GFP and CaM2–mCherry in tobacco leaves, red fluorescence from the latter protein was equally distributed between the cytosol and the nucleus and was localized near the plasma membrane (**Fig. 4E–H**). Thus, according to their physical vicinity, CaM2 and CNGC20 could interact in vivo.

To visualize this interaction, we used the split Venus interaction assay in *N. benthamiana* (Gehl et al. 2009). CNGC20 was fused either N- or C-terminally to the N-terminal part of the yellow fluorescent reporter Venus (VN = $Venus^N$), resulting in CNGC20–VN and VN–CNGC20, respectively. CaM2, CML8 and CML9 were added at the C-terminal side of the C-terminal part of Venus (VC = $Venus^C$). Following pairwise co-expression in

 © The Author 2013.

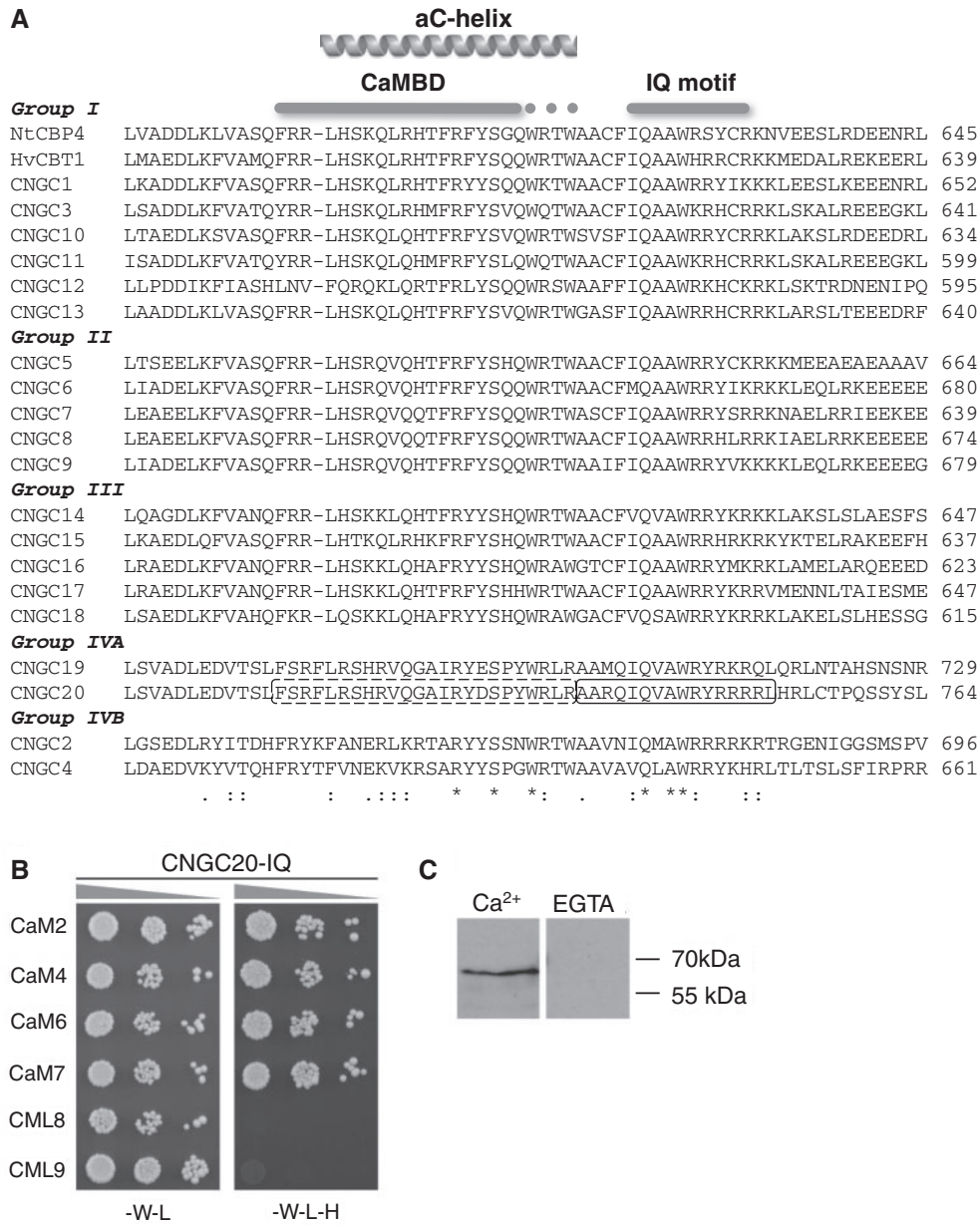

Fig. 3 The IQ domain mediates interaction of CNGC20 and CaMs. (A) Alignment of the C-terminal regions from 20 Arabidopsis CNGCs, the barley CaM-binding transporter HvCBT1 and tobacco CaM-binding protein NtCBP4, including its predicted αC-helix of the CNBD (Arazi et al. 2000) and two CaM-binding sites (gray bars): (i) the CaMBD (Köhler and Neuhaus 2000, Reddy et al. 2002) and the extended CaMBD (gray dots, Arazi et al. 2000), (ii) an IQ motif according to Bähler and Rhoads (2002; Abel et al., 2005). Boxes in the CNGC20 sequence show the peptides used for YTH, CNGC20-αC (dashed, see **Fig. 2**) and CNGC20-IQ (solid, see B). CNGCs are separated into five subgroups according to Mäser et al. (2001). (B) Interaction of the IQ domain of CNGC20 (CNGC20-IQ) and CaMs in a YTH assay as described in **Fig. 1**. (C) Ca^{2+}-dependent CaM binding to CNGC20-C was determined in a CaM overlay assay. Cell extracts of *E. coli* expressing CNGC20-C were separated by SDS–PAGE, subjected to Western blot and incubated with purified, Strep-tagged CaM2 in the presence of 5 mM $CaCl_2$ or in the absence of Ca^{2+} (5 mM EGTA). Strep-CaM2 interacting with CNGC20-C (MBP fusion: 62 kDa) was detected with an anti-Strep antibody.

tobacco leaves, the yellow fluorescence was compared for the different combinations. While bright yellow fluorescence was reported from epidermal cells upon co-expression of CNGC20–VN with VC–CaM2 (**Figs. 5A**, **6A**), it was reduced to background levels when the reporter was fused to the N-terminus of CNGC20 (VN–CNGC20, **Fig. 6C**). These results demonstrate that CNGC20 can recruit CaM2 to the plasma membrane. In order to compare the efficiency of interaction, we used CNGC20–VN for co-expression with VC–CaM2, VC–CML8 and VC–CML9. As judged from the fluorescence intensities obtained in parallel experiments (**Fig. 6A–H**), CML9 and CML8 were not or only very weakly able to interact with

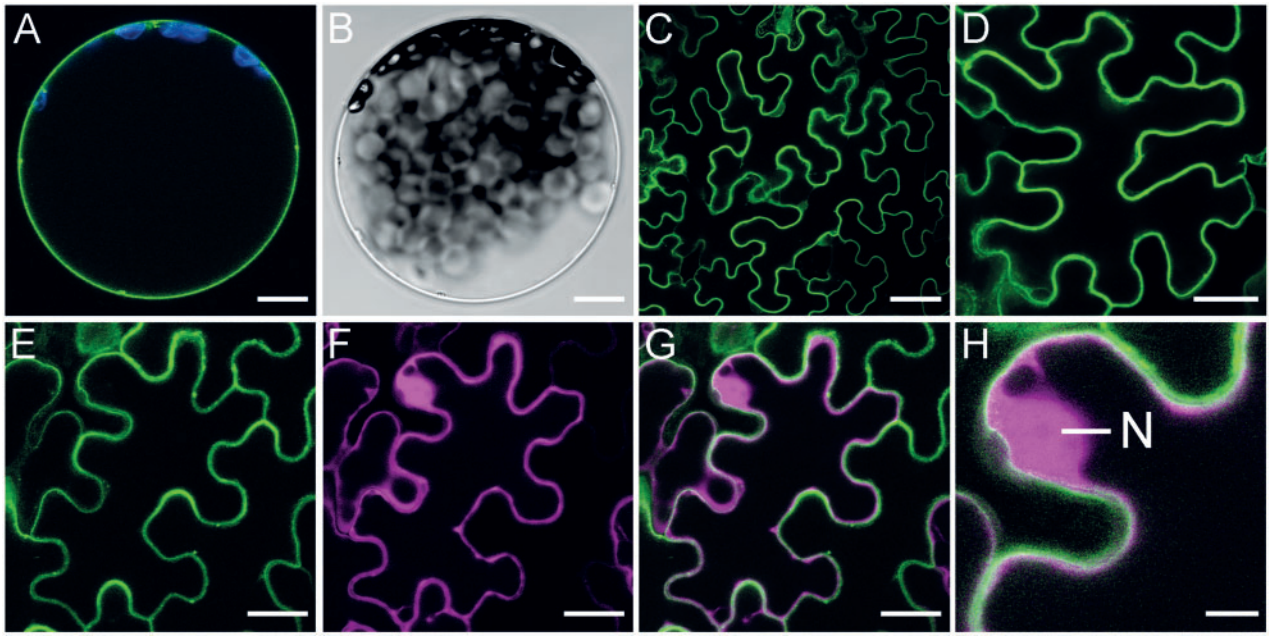

Fig. 4 Localization of CNGC20 and CaM2. Fluorescence of CNGC20 GFP fusion proteins in (A–H) is shown in green. (A and B) CNGC20–GFP expressed in *N. benthamiana* protoplasts. Chloroplast fluorescence is shown in blue. (B) Bright field image corresponding to A. (C–H) Tobacco epidermal cells expressing (C) CNGC20–GFP, (D) GFP–CNGC20 and (E–H) CNGC20–GFP in addition to CaM2–mCherry. mCherry fluorescence is shown in magenta. (E) Green fluorescence; (F) red fluorescence; (G) overlay image of (E) and (F); (H) higher magnified detail of (G). An N labels the position of the nucleus, where the nucleoli can be identified as areas of reduced fluorescence. Bars represent 10 μm (A, B), 50 μm (C), 30 μm (D), 20 μm (E–G) and 5 μm (H).

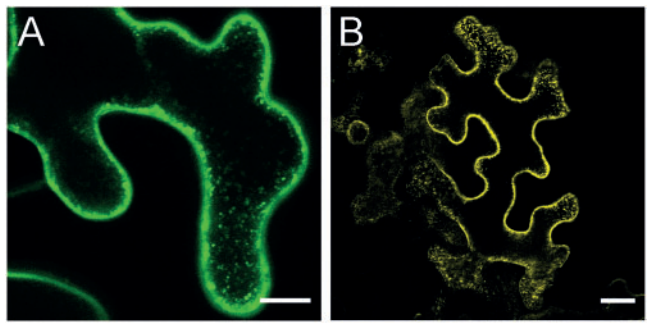

Fig. 5 Plasma membrane and intracellular GFP fluorescence of CNGC20GFP fusion proteins or BiFC signals from CNGC20 interaction with CaM. (A) GFP–CNGC20; (B) BiFC CNGC20–VN and VC–CaM2. All constructs were expressed in tobacco epidermal cells. Bars represent 10 μm (A) and 20 μm (B). In addition to the fluorescence at the plasma membrane, dots near the plasma membrane were often visible.

CNGC20, confirming the results from the YTH assay. Virtually no yellow fluorescence was observed after co-expression of CNGC20–VN with VC alone (**Fig. 6I**) or with bZIP63–VC (**Fig. 6K**), a transcription factor expected to localize to the nucleus (Walter et al. 2004).

In order to verify the interaction of the isolated C-terminus of CNGC20 and CaM in vivo, we conducted bimolecular fluorescence complementation (BiFC) assays, using only the C-terminal part of the channel (CNGC20-C). A BiFC signal was induced in the presence of CNGC20-C–VN and VC–CaM2 (**Fig. 7A**), which was weak in the presence of VC–CML8 (**Fig. 7C**) and virtually absent in the presence of VC–CML9 (**Fig. 7F**). This confirms the specificity of the interaction between CNGC20 and CaM. Interestingly, the proteins interacted mainly in the nucleus rather than in the cytosol (**Fig. 7A**, **D**). Since CaM2 was localized in the nucleus and in the cytosol (**Fig. 4F**), the question arose as to why the interaction with CNGC20-C was restricted to the nucleus.

A nuclear localization sequence within the IQ domain directs the C-terminus of CNGC20 into the nucleus

To monitor the cellular localization of the isolated C-terminal fragment of CNGC20 used before, we fused it N-terminally to GFP (CNGC20-C–GFP). CNGC20-C–GFP accumulated in the nucleus rather than in the cytosol of mesophyll protoplasts and epidermal cells (**Fig. 8A–D**). A nuclear localization sequence (NLS) of the type [YFW]RRRR[PL] is present within the IQ domain of the CNGC20 C-terminus (Rost et al. 2004). We therefore substituted the first three of four arginine residues within the NLS, and the resulting mutant CNGC20-C_{AAA}–GFP was analysed for its localization. Indeed, the absence of the NLS prevented nuclear accumulation of CNGC20-C_{AAA}–GFP, as concluded from the GFP fluorescence equilibrating between the nucleus and the cytosol (**Fig. 8E**, **F**). This shows that CNGC20 exhibits a functional NLS, which is part of the IQ

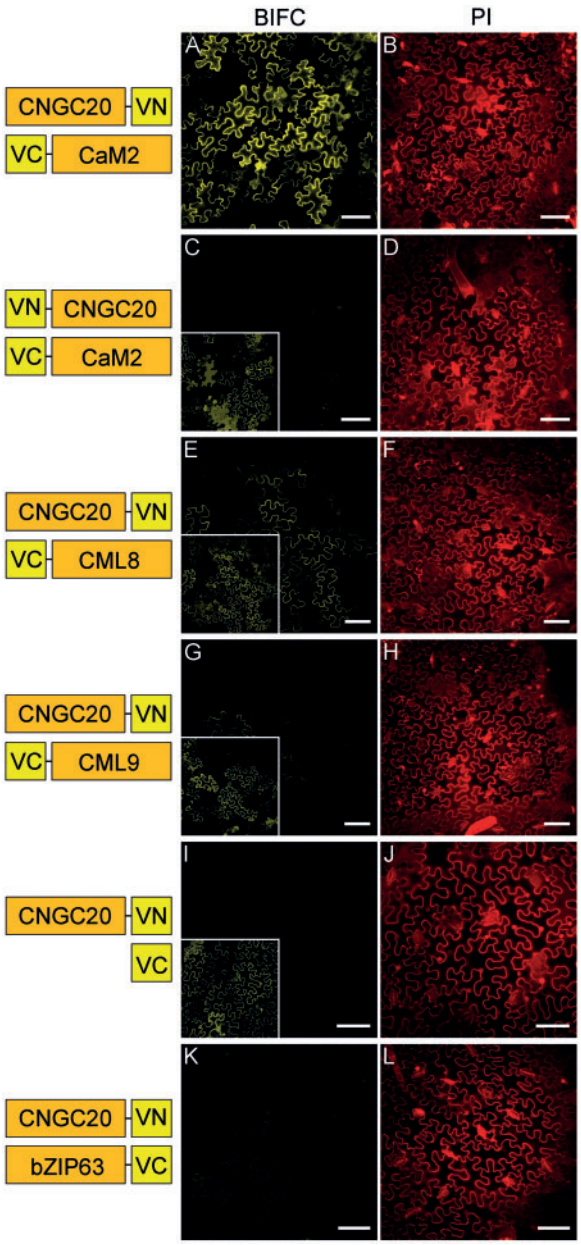

Fig. 6 CNGC20 interacts with CaM at the plasma membrane. (A–L) Images of BiFC signals (yellow, middle column) and propidium iodide (PI) staining (red, right column) in tobacco epidermal cells after co-expression of CNGC20 fused to the N-terminal part of Venus (VN) and the interaction partners fused to the C-terminal part of Venus (VC). Co-expression partners for each experiment are depicted in the left column. Bars represent 75 μm. Vector containing VC only (I) and bZIP63–VC (K) were used as negative controls. For comparison of the BiFC signal intensities, corresponding images were taken with the same laser intensities, photomultiplier settings and magnification, and were equally processed. Insets show the same images adjusted with different tonal values, brightness and contrast, in order to enhance the low signal intensities.

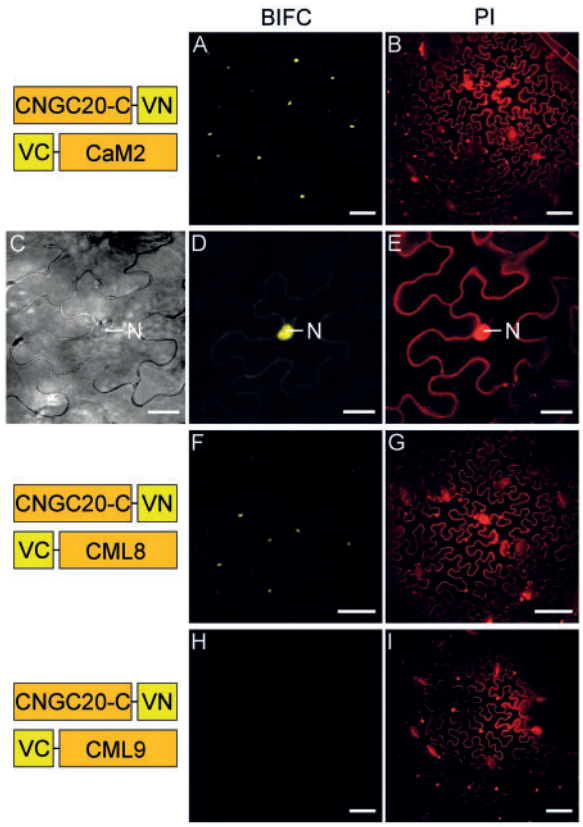

Fig. 7 The C-terminus of CNGC20 interacts with CaM in the nucleus. Layout and experimental set-up as described in **Fig. 6**. BiFC signals indicate the interaction between the C-terminus and CaM2 in the nucleus (A, D). (C–E) Co-expression partners as in (A) were used and corresponding images for bright field (C, trimmed width), BiFC signals (D) and PI staining (E) are shown at a higher magnification, where the nucleus is clearly detectable in each image. Bars represent 75 μm, and in (C–E) 20 μm.

domain. However, the NLS was not required for the targeting of the full-length channel, since GFP fusion proteins of CNGC20 lacking the IQ/NLS domain (CNGC20-ΔC34) reached the plasma membrane (**Fig. 8G**).

Together, our results identified two functional domains downstream of the CNBD (**Fig. 9**), an IQ domain, which binds CaM in a Ca^{2+}-dependent manner, and an embedded NLS, whose function for the full-length channel remains unclear.

Discussion

Here, we showed that a previously uncharacterized CaM-binding site operates in plant CNGCs and for the first time demonstrate interaction of these channels with CaM in planta. While several members of the CNGC family employ the αC-helix of the CNBD to bind CaM (**Fig. 3**; Kaplan et al. 2007), in CNGC20 we mapped a functional Ca^{2+}-dependent CaM-binding site C-terminal to the CNBD, which belongs to

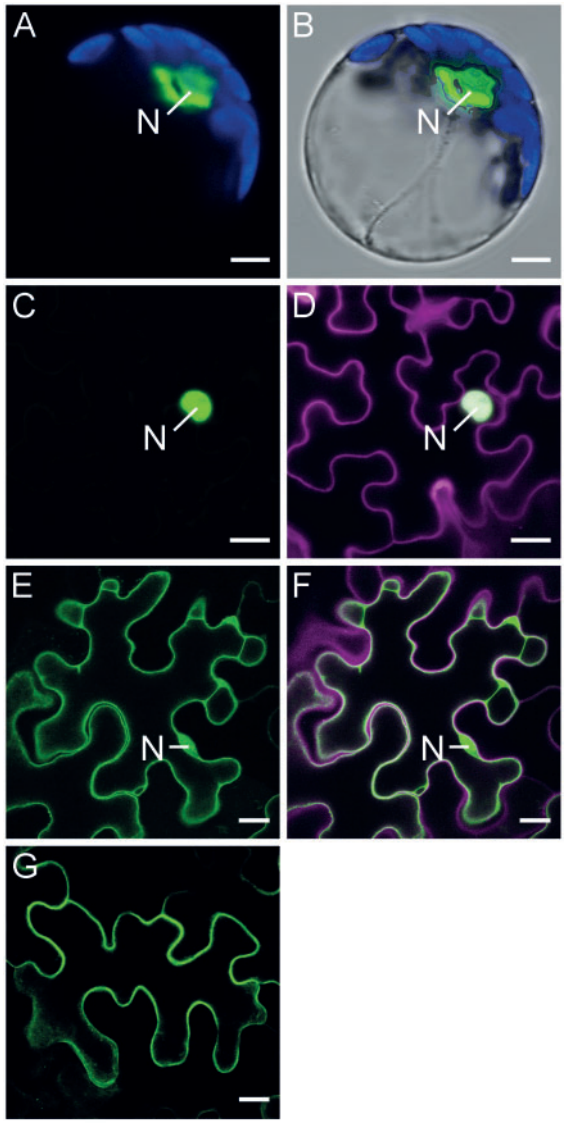

Fig. 8 An NLS directs the C-terminus of CNGC20 to the nucleus. (A and B) CNGC20-C–GFP expressed in tobacco mesophyll protoplasts. (A) GFP fluorescence is shown in green, chloroplast fluorescence in blue. (B) Overlay of fluorescence image shown in A and the corresponding bright field image. Bars respresent 5 µm. (C–F) CNGC20-C–GFP (C, D) and CNGC20-C_{AAA}–GFP with a mutated NLS (R748A/R749A/R750A) (E, F) expressed in tobacco epidermal cells. Bars represent 20 µm. (G) GFP–CNGC20ΔC34. Bar represents 25 µm. In (C–G) GFP fluorescence is shown in green, propidium iodide fluorescence in magenta. In (A–F) the nucleus is marked.

the IQ class of binding sites. CNGC20 is the first example for the IQ domain-mediated function in a plant transport protein. The IQ domain characterized here is conserved among plant CNGCs (**Fig. 3**), and IQ domains are present in, for example, several members of the glutamate receptor family of cation channels, in a V-type ATPase subunit, in boron as well as in phosphate transporters of Arabidopsis (ScanProsite Tool, de Castro et al. 2006). Embedded in the IQ domain of CNGC20 lies an NLS, the mutation of which impaired the otherwise observed nuclear accumulation of the isolated C-terminus of CNGC20 but did not abrogate plasma membrane localization of the full-length channel when it is missing (**Fig. 8**). The organization of the functional domains characterized in this and previous studies are illustrated together in **Fig. 9**.

NLS motifs are present in many different ion channels including glycine receptors, voltage-gated Ca^{2+} channels and *N*-methyl-D-aspartate receptors from animal cells (Holmes et al. 2002, Gomez-Ospina et al. 2006, Melzer et al. 2010). The NLS present in the neuronal voltage-gated Ca^{2+} channel, $Ca_V1.2$, was shown to mediate transfer of the C-terminal channel fragment to the nucleus after proteolytic cleavage, where it acts as a transcriptional regulator (Gomez-Ospina et al. 2006). We have not observed a nuclear signal from GFP C-terminally fused to CNGC20, and neither did we observe nuclear BiFC signals using the full-length channel and CaM2. Together, our data suggest the dominant function of CNGC20 to reside in the plasma membrane but cannot rule out the possibility of a so far unknown stimulus-specific channel cleavage and a role for the C-terminus in the nucleus. However, we can rule out a function of the NLS and IQ domain for targeting of CNGC20 to the plasma membrane. As the NLS forms part of the IQ domain, its role may be restricted to providing basic residues required for CaM binding. Alternatively, such basic residues have been shown to function as an arginine-based endoplasmic reticulum retrieval and retention signal (Zerangue et al. 2001, Michelsen et al. 2005).

The potential to form a basic amphipathic α-helix is a prerequisite for binding of the CaM ligand. The αC-helix of the CNBD in both NtCBP4 (FRR. . .WRTW, Arazi et al. 2000a) and CNGC1 (FRR. . .WKTW) fulfills these criteria by orienting the basic residues to one side of the helix, creating a high hydrophobic moment (Heliquest calculation, Gautier et al. 2008). In contrast, the homologous region in CNGC20 (FSR. . .WRLR) is characterized by a low hydrophobic moment, indicating that this region does not form an amphipathic helix. Instead, a high hydrophobic moment and positive net charge are found for the IQ domain (RQIQ. . .HRLC) of CNGC20, supporting our findings that CaM binds to the IQ domain rather than to a region within the CNBD.

Besides their role in subunit assembly and trafficking, IQ domains are involved in Ca^{2+}-dependent regulation of channel activity (Zühlke et al. 2000, Etxeberria et al. 2008, Mruk et al. 2012). Often, Ca^{2+} channels employ CaM as the sensor for changes in Ca^{2+} concentration, which is used for self-regulation, in order to shape the spatial and time-dependent Ca^{2+} signal, which in turn activates a stimulus-specific response (Dunlap 2007). The presence of two different types of CaMBDs in plant CNGCs highlights similarities to the voltage-dependent Ca^{2+} channels from animal cells (Pitt et al. 2001) and furthermore suggests that the two domains serve different functions. For gating control of plant CNGCs, Ca^{2+}/CaM binding to the CaMBD has been proposed to compete directly with the binding of cyclic nucleotides to the overlapping CNBD (Arazi et al. 2000a, Kaplan et al. 2007), suggesting that this site is involved in

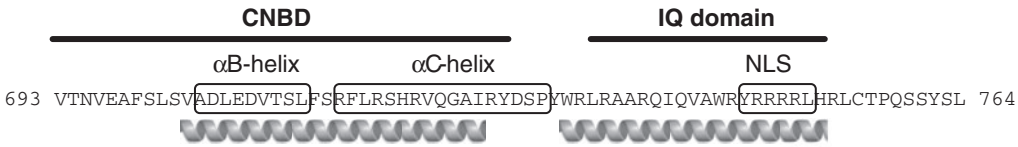

Fig. 9 Model of the domain architecture in CNGC20. The CNBD (593–728) in part and the IQ domain are shown according to domain homologies (Bähler and Rhoads 2002, Letunic et al. 2012). The αB- and αC-helix of the CNBD are annotated from sequence homology to human CNGCs and HCN channels (Zagotta et al. 2003, Cukkemane et al. 2011). The NLS is highlighted, and predicted α-helical secondary structures for CNGC20 (Buchan et al. 2010) are illustrated below the sequence.

the Ca^{2+}-dependent desensitization process. In contrast, binding of CaM to the IQ domain is not necessarily associated with the displacement of the ligand from the CNBD. Similar to the mammalian CNGB1, this site may function in recruiting CaM to the channel via one part of the IQ domain under resting conditions, which in turn can interact in a Ca^{2+}-dependent manner with the second part of the IQ domain, resulting in conformational changes and reduced channel activity (Trudeau et al. 2004, Ungerer et al. 2011). In heteromeric complexes, channel-bound CaM may also interact with a CaMBD of another subunit. As shown for mammalian CNGCs and voltage-dependent Ca^{2+} channels (Dunlap 2007, Ungerer et al. 2011), such a close association of CaM with its target under resting conditions would serve as a built-in sensor for Ca^{2+} passing through the channel pore, which enables fast and sensitive feedback regulation.

Arabidopsis expresses five different CaM isoforms (Gawienowski et al. 1993, Reddy et al. 2002, McCormack et al. 2005). While loss of different CaM isoforms induces unique phenotypes (Perochon et al. 2011), we have shown that CNGC20 is able to bind to all CaM isoforms, implicating that this channel may be addressed during the responses to different physiological stimuli, such as salt stress or pathogen attack. In contrast, other CNGC subunits discriminate moderately or strongly between the different CaM isoforms (Köhler et al. 2000, authors' own unpublished observations). Depending on the expression, subcellular distribution and affinity of CaM isoforms for CNGCs, these Ca^{2+} sensors play important roles, both in shaping of a Ca^{2+} response mediated by CNGCs, and in decoding the Ca^{2+} signature for stimulus-specific downstream responses.

In summary, our results implicate a more complex CNGC regulation as compared with the competitive ligand-binding model and further underline the functional diversity within this gene family. Depending on the subunit composition, gating modes and cellular functions of plant CNGCs may thus be even more diverse than previously expected. In this context, it has recently been shown that the absence of *CNGb* from *Physcomitrella patens* results in an increased heat-stimulated Ca^{2+} response (Finka et al. 2012). Although the underlying mechanism is not fully understood, the loss of a channel subunit with unique CaM-binding characteristics may indeed alter the Ca^{2+}-dependent feedback control of residual CNGCs. It will therefore be of prime importance to determine the CaM-binding properties of the individual CNGC subunits qualitatively and quantitatively in detail and investigate the cell- and tissue-specific stoichiometry of functional channels, in order to determine their physiological function in a specific Ca^{2+} signaling network.

Materials and Methods

Plant material and transformation

Nicotiana benthamiana (tobacco) was grown on soil in the green house.

For transient expression in leaves of 6- to 8-week-old *N. benthamiana* (Voinnet et al. 2003, Walter et al. 2004), *Agrobacterium* strain C58C1 carrying the plasmid of interest and the helper strain p19 were grown overnight in YEB medium (0.5% tryptone, 0.5% yeast extract, 0.5% sucrose, 50 mM $MgSO_4$, pH 7.8) at 29°C. Cells were harvested and resuspended to an OD_{600} of 1 in infiltration buffer [10 mM MES, pH 5.7 (KOH), 10 mM $MgCl_2$, 100 μM acetosyringone]. The *Agrobacterium* C58C1 suspension was mixed with 1 vol. of the p19 helper strain (Voinnet et al. 2003), incubated for 3 h and injected into the abaxial side of tobacco leaves. For co-expression of two proteins, the plasmid-carrying agrobacteria were mixed in equal amounts before addition of the p19 helper strain.

Construction of plasmids

Gateway-compatible PCR products of CNGC20 (At3g17700), CaM2 (At2g41110), CaM4 (At1g66410), CaM6 (At5g21274), CaM7 (At3g43810), CML8 (At4g14640) and CML9 (At3g51920) were produced using primers 1–27 listed in **Supplementary Table S2** and ligated into the pENTR/D-TOPO vector (Invitrogen). CaM2/pENTR/SD/D-TOPO (U17248) was ordered from the ABRC stock center. These genes were integrated into gateway destination vectors using LR clonase (Invitrogen). For YTH studies, the constucts used as bait were recombined into pGBT9-GW and prey constructs into pGAD424-GW, kindly provided by F. Börnke, Erlangen University. pVYNE, pVYNE(R) and pVYCE(R) (Gehl et al. 2009) were used for BiFC assays. For N-terminal GFP fusions, the pMDC43 destination vector was used (Curtis et al. 2003). A C-terminal GFP fusion was achieved using the destination vector pK7FWG2,0 (Karimi et al. 2002). For C-terminal mCherry fusions, pMDC201-mCherry was produced by a replacement of GFP by mCherry. mCherry was kindly provided by R. Stadler

(Erlangen Universiy). Restriction sites *Asc*I and *Bst*BI were added to mCherry by an amplification using primers 28 and 29 (**Supplementary Table S2**) and the digested fragment was used to substitute the GFP in pMDC201 (Curtis et al. 2003). For a maltose-binding protein (MBP) fusion to the CNGC20 C-terminus, the latter was amplified with primers 30 and 31 and introduced into pMal-c2x (New England Biolabs) via *Xmn*I and *Hin*dIII. Strep-CaM2 fusion was generated by an amplification of CaM2 with primers 32 and 33 and cloning into pASK-IBA5plus (IBA BioTAGnology) via *Bam*HI and *Pst*I. For insertion of a mutation into the NLS, primers 34 and 35 and the Quick Change II Site-Directed Mutagenesis Kit (Stratagene) were used following the manufacturer's instructions.

Yeast two-hybrid assays

The CNGC20 variants were fused to the GAL4 DNA-binding domain in pGBT9-GW. CaMs and CMLs were cloned into the pGAD424-GW vector for a fusion with the GAL4 activation domain. All constructs were produced using the gateway cloning strategy (Invitrogen). Gateway-compatible YTH vectors were kindly provided by F. Börnke (Erlangen University). The yeast strain AH109 (Clontech Laboratories Inc.) was co-transformed with pairs of each combination of pGBT9 and pGAD424 vectors, and also with empty vectors, and selected for co-transformed cells on plates lacking tryptophan and leucine (−W, −L). Transformed cells were grown in liquid selection media (−W, −L), adjusted to an OD_{600} of 2, 0.2 and 0.02, and 5 µl of each concentration were spotted on selection plates with (−W, −L) and without histidine (−W, −L, −H). Plates were grown at 29°C for 3 d. *o*-Nitrophenyl-β-galactoside (ONPG) assays were performed following the Clontech protocol.

The following CNGC20 fragments were used in YTH assays: CNGC20-C (corresponding to $CNGC20_{517-764}$); CNGC20-C-ΔC63 ($CNGC20_{517-701}$); CNGC20-C-ΔC34 ($CNGC20_{517-730}$); CNGC20-CC ($CNGC20_{730-764}$); CNGC20-αBC ($CNGC20_{698-731}$); CNGC20-αC ($CNGC20_{713-736}$); and CNGC20-IQ ($CNGC20_{737-752}$).

Recombinant protein expression, purification and calmodulin overlay assay

Strep-CaM2 was expressed in *Escherichia coli* SoluBL21 cells (AMS Biotechnology) by 4 h induction with 1 µg ml^{-1} doxycycline at 37°C in the dark. The Strep-CaM2 protein was purified using a StrepTactin column (IBA BioTAGnology), following the instructions of the manufacturer. *Escherichia coli* SoluBL21 cells were transformed with pMAL-c2x harboring *MBP-CNGC20-C*, and protein expression was induced by 2 mM isopropyl-β-D-thiogalactopyranoside (IPTG) at 37°C for 3 h. Proteins were separated by SDS–PAGE, followed by transfer onto a polyvinylidene difluoride membrane. The membrane was cut in two halves, each containing MBP–CNGC20-C. The membranes were blocked with buffer (0.1 M NaCl, 50 mM Tris–HCl, pH 7.5, 1 mg ml^{-1} bovine serum albumin, 0.05% Tween-20) containing either 5 mM Ca^{2+} or 5 mM EGTA for 30 min. For CaM binding, the membranes were incubated with purified Strep-CaM2 diluted in the same buffer to a final concentration of 0.1 µg ml^{-1}. After washing in the above buffer, the membranes were incubated overnight with an anti-Strep antibody (IBA BioTAGnology), diluted 1:2,500 in the above buffer. CaM2 binding was detected using a horseradish peroxidase-coupled anti-mouse IgG (Sigma-Aldrich) and the Lumi-Light western blotting kit (Roche).

BiFC assays

Gateway-compatible plasmids for BiFC analysis were kindly provided by Jörg Kudla (University of Muenster). For a BiFC assay, agrobacteria harboring plasmids with Venus N- and C-terminal fusions were mixed 1:1 before an equal amount of p19 was added to the suspension. At 2–3 d following infiltration of agrobacteria into tobacco, leaf discs were prepared for microscopic analysis. To compare fluorescence intensity between samples, these pictures were taken with the same laser intensities, photomultiplier settings and at the same magnification.

Confocal microscopy

Confocal laser scanning microscopy (Leica TCS SP II; Leica Microsystems) was used with laser excitation at 488 nm for GFP, mCherry and propidium iodide (PI), and at 514 nm for Venus. Detection windows were set from 500 to 540 nm for GFP, from 530 to 550 nm for Venus, from 650 to 770 nm for mCherry and from 615 to 665 nm for PI. Cell walls were stained with PI for about 15 min and washed with water prior to confocal fluorescence imaging.

Supplementary data

Supplementary data are available at PCP online

Funding

This work was supported by the Deutsche Forschungsgemeinschaft [FOR964 grant to P.D.].

Acknowledgments

We would like to thank Heinrich Sticht (Erlangen University) for helpful discussion about structural requirements for CaM binding. We thank Tanja Bender and Joanna Urbaniak-Bogdanska (Erlangen University) for excellent technical assistance, and Nadine Rehm (Erlangen University) for help with protein purification. We are grateful to Norbert Sauer for sharing the confocal microscopy facility.

References

Abel, S., Savchenko, T. and Levy, M. (2005) Genome-wide comparative analysis of the IQD gene families in *Arabidopsis thaliana* and *Oryza sativa*. *BMC Evol. Biol.* 5: 72.

Arazi, T., Kaplan, B. and Fromm, H. (2000a) A high-affinity calmodulin-binding site in a tobacco plasma-membrane channel protein coincides with a characteristic element of cyclic nucleotide-binding domains. *Plant Mol. Biol.* 42: 591–601.

Arazi, T., Kaplan, B., Sunkar, R. and Fromm, H. (2000b) Cyclic-nucleotide- and Ca^{2+}/calmodulin-regulated channels in plants: targets for manipulating heavy-metal tolerance, and possible physiological roles. *Biochem. Soc. Trans.* 28: 471–475.

Ascencio-Ibanez, J.T., Sozzani, R., Lee, T.J., Chu, T.M., Wolfinger, R.D., Cella, R. et al. (2008) Global analysis of Arabidopsis gene expression uncovers a complex array of changes impacting pathogen response and cell cycle during geminivirus infection. *Plant Physiol.* 148: 436–454.

Bähler, M. and Rhoads, A. (2002) Calmodulin signaling *via* the IQ motif. *FEBS Lett.* 513: 107–113.

Bouché, N., Yellin, A., Snedden, W.A. and Fromm, H. (2005) Plant-specific calmodulin-binding proteins. *Annu. Rev. Plant Biol.* 56: 435–466.

Buchan, D.W., Ward, S.M., Lobley, A.E., Nugent, T.C., Bryson, K. and Jones, D.T. (2010) Protein annotation and modelling servers at University College London. *Nucleic Acids Res.* 38: W563–W568.

Chan, C.W., Schorrak, L.M., Smith, R.K. Jr, Bent, A.F. and Sussman, M.R. (2003) A cyclic nucleotide-gated ion channel, CNGC2, is crucial for plant development and adaptation to calcium stress. *Plant Physiol.* 132: 728–731.

Chin, K., Moeder, W. and Yoshioka, K. (2009) Biological roles of cyclic-nucleotide-gated ion channels in plants: what we know and don't know about this 20 member ion channel family. *Botany* 87: 668–677.

Christopher, D.A., Borsics, T., Yuen, C.Y., Ullmer, W., Andeme-Ondzighi, C., Andres, M.A. et al. (2007) The cyclic nucleotide gated cation channel AtCNGC10 traffics from the ER *via* Golgi vesicles to the plasma membrane of Arabidopsis root and leaf cells. *BMC Plant Biol.* 7: 48.

Clough, S.J., Fengler, K.A., Yu, I.C., Lippok, B., Smith, R.K. Jr and Bent, A.F. (2000) The *Arabidopsis dnd1* 'defense, no death' gene encodes a mutated cyclic nucleotide-gated ion channel. *Proc. Natl Acad. Sci. USA* 97: 9323–9328.

Cukkemane, A., Seifert, R. and Kaupp, U.B. (2011) Cooperative and uncooperative cyclic-nucleotide-gated ion channels. *Trends Biochem. Sci.* 36: 55–64.

Curtis, M.D. and Grossniklaus, U. (2003) A gateway cloning vector set for high-throughput functional analysis of genes in planta. *Plant Physiol.* 133: 462–469.

de Castro, E., Sigrist, C.J., Gattiker, A., Bulliard, V., Langendijk-Genevaux, P.S., Gasteiger, E. et al. (2006) ScanProsite: detection of PROSITE signature matches and ProRule-associated functional and structural residues in proteins. *Nucleic Acids Res.* 34: W362–W365.

DeFalco, T.A., Bender, K.W. and Snedden, W.A. (2010) Breaking the code: Ca^{2+} sensors in plant signalling. *Biochem. J.* 425: 27–40.

Dietrich, P., Anschütz, U., Kugler, A. and Becker, D. (2010) Physiology and biophysics of plant ligand-gated ion channels. *Plant Biol.* 12: 80–93.

Dodd, A.N., Kudla, J. and Sanders, D. (2010) The language of calcium signaling. *Annu. Rev. Plant Biol.* 61: 593–620.

Dunlap, K. (2007) Calcium channels are models of self-control. *J. Gen. Physiol.* 129: 379–383.

Etxeberria, A., Aivar, P., Rodriguez-Alfaro, J.A., Alaimo, A., Villace, P., Gomez-Posada, J.C. et al. (2008) Calmodulin regulates the trafficking of KCNQ2 potassium channels. *FASEB J.* 22: 1135–1143.

Finka, A., Cuendet, A.F., Maathuis, F.J., Saidi, Y. and Goloubinoff, P. (2012) Plasma membrane cyclic nucleotide gated calcium channels control land plant thermal sensing and acquired thermotolerance. *Plant Cell* 24: 3333–3348.

Gautier, R., Douguet, D., Antonny, B. and Drin, G. (2008) HELIQUEST: a web server to screen sequences with specific alpha-helical properties. *Bioinformatics* 24: 2101–2102.

Gawienowski, M.C., Szymanski, D., Perera, I.Y. and Zielinski, R.E. (1993) Calmodulin isoforms in Arabidopsis encoded by multiple divergent mRNAs. *Plant Mol. Biol.* 22: 215–225.

Gehl, C., Waadt, R., Kudla, J., Mendel, R.R. and Hansch, R. (2009) New GATEWAY vectors for high throughput analyses of protein–protein interactions by bimolecular fluorescence complementation. *Mol. Plant.* 2: 1051–1058.

Gomez-Ospina, N., Tsuruta, F., Barreto-Chang, O., Hu, L. and Dolmetsch, R. (2006) The C terminus of the L-type voltage-gated calcium channel Ca(V)1.2 encodes a transcription factor. *Cell* 127: 591–606.

Hammes, U.Z., Schachtman, D.P., Berg, R.H., Nielsen, E., Koch, W., McIntyre, L.M. et al. (2005) Nematode-induced changes of transporter gene expression in Arabidopsis roots. *Mol. Plant-Microbe Interact.* 18: 1247–1257.

Holmes, K.D., Mattar, P., Marsh, D.R., Jordan, V., Weaver, L.C. and Dekaban, G.A. (2002) The C-terminal C1 cassette of the N-methyl-D-aspartate receptor 1 subunit contains a bi-partite nuclear localization sequence. *J. Neurochem.* 81: 1152–1165.

Hua, B.G., Mercier, R.W., Zielinski, R.E. and Berkowitz, G. (2003) Functional interaction of calmodulin with a plant cyclic nucleotide gated cation channel. *Plant Physiol. Biochem.* 41: 945–954.

Kanter, U., Hauser, A., Michalke, B., Draxl, S. and Schaffner, A.R. (2010) Caesium and strontium accumulation in shoots of Arabidopsis thaliana: genetic and physiological aspects. *J. Exp. Bot.* 61: 3995–4009.

Kaplan, B., Sherman, T. and Fromm, H. (2007) Cyclic nucleotide-gated channels in plants. *FEBS Lett.* 581: 2237–2246.

Karimi, M., Inze, D. and Depicker, A. (2002) GATEWAY vectors for Agrobacterium-mediated plant transformation. *Trends Plant Sci.* 7: 193–195.

Kilian, J., Whitehead, D., Horak, J., Wanke, D., Weinl, S., Batistic, O. et al. (2007) The AtGenExpress global stress expression data set: protocols, evaluation and model data analysis of UV-B light, drought and cold stress responses. *Plant J.* 50: 347–363.

Köhler, C. and Neuhaus, G. (2000) Characterisation of calmodulin binding to cyclic nucleotide-gated ion channels from *Arabidopsis thaliana*. *FEBS Lett.* 471: 133–136.

Kugler, A., Köhler, B., Wolff, P., Palme, K. and Dietrich, P. (2009) Salt-dependent regulation of a CNG channel subfamily in Arabidopsis. *BMC Plant Biol.* 9: 140–151.

Leba, L.J., Cheval, C., Ortiz-Martin, I., Ranty, B., Beuzon, C.R., Galaud, J.P. et al. (2012) CML9, an Arabidopsis calmodulin-like protein, contributes to plant innate immunity through a flagellin-dependent signalling pathway. *Plant J.* 71: 976–989.

Letunic, I., Doerks, T. and Bork, P. (2012) SMART 7: recent updates to the protein domain annotation resource. *Nucleic Acids Res.* 40: D302–D305.

Magnan, F., Ranty, B., Charpenteau, M., Sotta, B., Galaud, J.P. and Aldon, D. (2008) Mutations in AtCML9, a calmodulin-like protein from Arabidopsis thaliana, alter plant responses to abiotic stress and abscisic acid. *Plant J.* 56: 575–589.

Mäser, P., Thomine, S., Schroeder, J.I., Ward, J.M., Hirschi, K., Sze, H. et al. (2001) Phylogenetic relationships within cation transporter families of Arabidopsis. *Plant Physiol.* 126: 1646–1667.

McCormack, E. and Braam, J. (2003) Calmodulins and related potential calcium sensors of Arabidopsis. *New Phytol.* 159: 585–598.

McCormack, E., Tsai, Y.C. and Braam, J. (2005) Handling calcium signaling: Arabidopsis CaMs and CMLs. *Trends Plant Sci.* 10: 383–389.

Melzer, N., Villmann, C., Becker, K., Harvey, K., Harvey, R.J., Vogel, N. et al. (2010) Multifunctional basic motif in the glycine receptor intracellular domain induces subunit-specific sorting. *J. Biol. Chem.* 285: 3730–3739.

Michelsen, K., Yuan, H. and Schwappach, B. (2005) Hide and run. Arginine-based endoplasmic-reticulum-sorting motifs in the assembly of heteromultimeric membrane proteins. *EMBO Rep.* 6: 717–722.

Mruk, K., Shandilya, S.M., Blaustein, R.O., Schiffer, C.A. and Kobertz, W.R. (2012) Structural insights into neuronal K^+ channel–calmodulin complexes. *Proc. Natl Acad. Sci. USA* 109: 13579–13583.

O'Neil, K.T. and DeGrado, W.F. (1990) How calmodulin binds its targets: sequence independent recognition of amphiphilic alpha-helices. *Trends Biochem. Sci.* 15: 59–64.

Pate, P., Mochca-Morales, J., Wu, Y., Zhang, J.Z., Rodney, G.G., Serysheva, I.I. et al. (2000) Determinants for calmodulin binding on voltage-dependent Ca^{2+} channels. *J. Biol. Chem.* 275: 39786–39792.

Perochon, A., Aldon, D., Galaud, J.P. and Ranty, B. (2011) Calmodulin and calmodulin-like proteins in plant calcium signaling. *Biochimie* 93: 2048–2053.

Peterson, B.Z., DeMaria, C.D., Adelman, J.P. and Yue, D.T. (1999) Calmodulin is the Ca^{2+} sensor for Ca^{2+}-dependent inactivation of L-type calcium channels. *Neuron* 22: 549–558.

Pitt, G.S., Zuhlke, R.D., Hudmon, A., Schulman, H., Reuter, H. and Tsien, R.W. (2001) Molecular basis of calmodulin tethering and Ca^{2+}-dependent inactivation of L-type Ca^{2+} channels. *J. Biol. Chem.* 276: 30794–30802.

Popescu, S.C., Popescu, G.V., Bachan, S., Zhang, Z., Seay, M., Gerstein, M. et al. (2007) Differential binding of calmodulin-related proteins to their targets revealed through high-density Arabidopsis protein microarrays. *Proc. Natl Acad. Sci. USA* 104: 4730–4735.

Reddy, V.S., Ali, G.S. and Reddy, A.S. (2002) Genes encoding calmodulin-binding proteins in the Arabidopsis genome. *J. Biol. Chem.* 277: 9840–9852.

Rhoads, A.R. and Friedberg, F. (1997) Sequence motifs for calmodulin recognition. *FASEB J.* 11: 331–340.

Rost, B., Yachdav, G. and Liu, J. (2004) The PredictProtein server. *Nucleic Acids Res.* 32: W321–W326.

Sanders, D., Pelloux, J., Brownlee, C. and Harper, J.F. (2002) Calcium at the crossroads of signaling. *Plant Cell.* 14(Suppl), S401–S417.

Schuurink, R.C., Shartzer, S.F., Fath, A. and Jones, R.L. (1998) Characterization of a calmodulin-binding transporter from the plasma membrane of barley aleurone. *Proc. Natl Acad. Sci. USA* 95: 1944–1949.

Trudeau, M.C. and Zagotta, W.N. (2004) Dynamics of Ca^{2+}-calmodulin-dependent inhibition of rod cyclic nucleotide-gated channels measured by patch-clamp fluorometry. *J. Gen. Physiol.* 124: 211–223.

Ungerer, N., Mücke, N., Broecker, J., Keller, S., Frings, S. and Möhrlen, F. (2011) Distinct binding properties distinguish LQ-type calmodulin-binding domains in cyclic nucleotide-gated channels. *Biochemistry* 50: 3221–3228.

Voinnet, O., Rivas, S., Mestre, P. and Baulcombe, D. (2003) An enhanced transient expression system in plants based on suppression of gene silencing by the p19 protein of tomato bushy stunt virus. *Plant J.* 33: 949–956.

Walter, M., Chaban, C., Schutze, K., Batistic, O., Weckermann, K., Nake, C. et al. (2004) Visualization of protein interactions in living plant cells using bimolecular fluorescence complementation. *Plant J.* 40: 428–438.

Winter, D., Vinegar, B., Nahal, H., Ammar, R., Wilson, G.V. and Provart, N.J. (2007) An 'Electronic Fluorescent Pictograph' browser for exploring and analyzing large-scale biological data sets. *PLoS One* 2: e718.

Yamniuk, A.P. and Vogel, H.J. (2004) Calmodulin's flexibility allows for promiscuity in its interactions with target proteins and peptides. *Mol. Biotechnol.* 27: 33–57.

Yu, I., Fengler, K.A., Clough, S.J. and Bent, A.F. (2000) Identification of *Arabidopsis* mutants exhibiting an altered hypersensitive response in gene-for-gene disease resistance. *Mol. Plant-Microbe Interact.* 13: 277–286.

Zagotta, W.N., Olivier, N.B., Black, K.D., Young, E.C., Olson, R. and Gouaux, E. (2003) Structural basis for modulation and agonist specificity of HCN pacemaker channels. *Nature* 425: 200–205.

Zerangue, N., Malan, M.J., Fried, S.R., Dazin, P.F., Jan, Y.N., Jan, L.Y. et al. (2001) Analysis of endoplasmic reticulum trafficking signals by combinatorial screening in mammalian cells. *Proc. Natl Acad. Sci. US.* 98: 2431–2436.

Zühlke, R.D., Pitt, G.S., Tsien, R.W. and Reuter, H. (2000) Ca^{2+}-sensitive inactivation and facilitation of L-type Ca^{2+} channels both depend on specific amino acid residues in a consensus calmodulin-binding motif in the (alpha)1C subunit. *J. Biol. Chem.* 275: 21121–21129.